Available online at www.sciencedirect.com

jmr&t Journal of Materials Research and Technology

www.jmrt.com.br

Original Article

TEM study of the effect of high-temperature thermal cycles on the stability of the Y-Al-O oxides in MA956 ODS steel

J.R.O. Leo[a,*,1], S.R. Moturu[a,2], M.E. Fitzpatrick[b]

[a] Materials Engineering, The Open University, Walton Hall, Milton Keynes MK7 6AA, UK
[b] Faculty of Engineering, Environment and Computing, Coventry University, Priory Street, Coventry CV1 5FB, UK

ARTICLE INFO

Article history:
Received 8 January 2019
Accepted 18 June 2019
Available online 11 July 2019

Keywords:
MA956
ODS
Characterization
Oxides
Heat treatment
TEM

ABSTRACT

MA956, a commercial ferritic grade of Oxide-Dispersion-Strengthened (ODS) steel, was investigated using transmission electron microscopy (TEM) to evaluate the influence of high-temperature thermal cycles on the nanometric dispersed oxides. Analyses of the oxide size distribution were carried out on foils from the as-received MA956 and following treatment at 1285 °C for one hour, and show that growth of the oxides has occurred under the thermal cycle. Implications for the oxide stability in the steel matrix are discussed, in the light of the oxide chemical composition.

© 2019 The Authors. Published by Elsevier B.V. This is an open access article under the CC BY-NC-ND license (http://creativecommons.org/licenses/by-nc-nd/4.0/).

1. Introduction

Incoloy alloy MA956 is a commercial oxide-dispersion strengthened (ODS) steel with a ferritic matrix [1]. It is an FeCrAl alloy system, whose composition aims at high oxidation resistance. The high content of chromium (20% wt.) and aluminium (5% wt.) in the matrix causes the formation of an adherent, slow-growing alumina scale that provides superior resistance to aggressive environments and high-temperature oxidation [2]. The alloy exhibits outstanding strength at temperatures over 1000 °C, owing to the fine dispersoids resulting from the formation of complex Y-Al-O oxides, homogeneously distributed through the matrix [3].

Previous investigations on a variety of ODS steels that were concerned with the size of the nanodispersoids for strengthening revealed higher stability than age-hardening precipitates, along with insolubility in the matrix at temperatures near the melting point of the base alloy [4,5]. While the chemical nature of the oxide has not been of primary concern, a number of studies investigated the effect of alloying elements on the refinement and on the formation of complex oxide particles [6–8], during processing of the alloys. However, no direct investigation has been carried out on the stability of the oxides after manufacturing. This work concentrates on

* Corresponding author.
E-mail: ac2452@coventry.ac.uk (J. Leo).
[1] Presently at Coventry University.
[2] Presently at Strathclyde University.

https://doi.org/10.1016/j.jmrt.2019.06.027

2238-7854/© 2019 The Authors. Published by Elsevier B.V. This is an open access article under the CC BY-NC-ND license (http://creativecommons.org/licenses/by-nc-nd/4.0/).

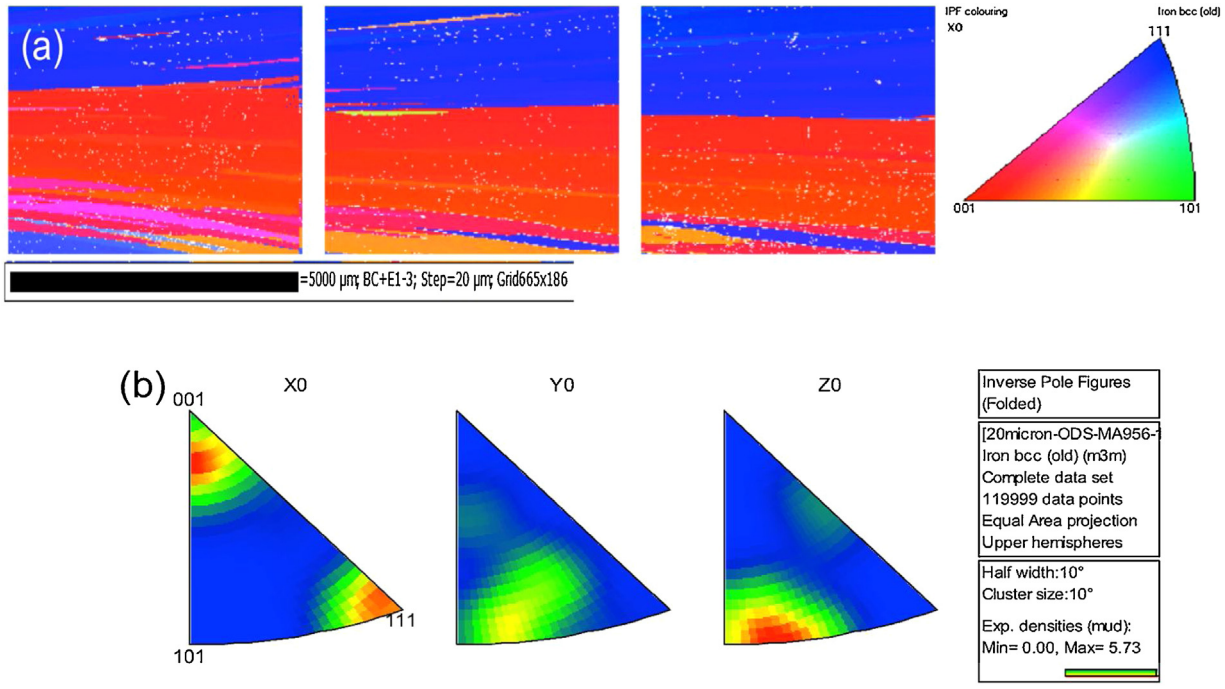

Fig. 1 – (a) EBSD maps of MA956 grains in the longitudinal direction, and (b) the corresponding IPF maps showing the predominant fibres, especially in the rolling direction (X0).

Table 1 – Chemical composition of the MA956 steel.

Cr	Al	Ti	Yttria	C	N	Mn	Si
19.4	4.8	0.38	0.51	0.015	0.022	0.10	0.04
Ni	**Cu**	**S**	**P**	**Co**	**O**	**Fe**	
0.05	0.02	0.008	0.005	<0.01	0.23	Bal.	

the evaluation of the stability of the Y-Al-O complex oxides of the MA956 subject to thermal processing following manufacturing.

2. Experimental Approach

MA956 material was supplied by Incotest (a Division of Special Metals Wiggin LTD), UK. Cylindrical samples with 16 mm diameter and 100 mm length were cut from the as-received hot-extruded bars. Chemical composition was provided by the manufacturer, as shown in Table 1.

Characterization of the material in the as-received condition was carried out by scanning electron microscopy with electron backscatter diffraction (SEM/EBSD) and transmission electron microscopy. Samples were extracted from both the cross-section (perpendicular to the bar axis) and longitudinal (along the bar axis) directions.

The preparation for EBSD involved grinding with SiC paper, polishing with diamond particles suspension (1 μm and 6 μm); and a final polishing stage with colloidal silica suspension OP-S, which consists of silicon oxide particles of sub-micron size range (<0.1 μm) in an alkaline medium, in order to achieve the polished surface finish. Cross-sectional and longitudinal samples were EBSD-scanned using step sizes of 5 μm and 20 μm, respectively.

For the TEM survey, three foils were prepared by manual grinding with SiC papers of 40, 15 and 5 μm, cut into a 3-mm-diameter disk and, then, further thinned by jet electropolishing in a solution of 5% perchloric acid and 95% ethanol at –50 °C. Imaging was conducted in bright-field mode (BF) in a JEOL JEM 2100 TEM to study the size distribution of the oxides. A total of 449 oxide particles were counted and measured from eight different micrographs, obtained by varying the area of the foil under investigation as well as the tilt angle of the specimen holder, in order to be statistically representative.

In its as-received condition, the MA956 contains high residual stresses, and mechanical tests showed poor ductility. Based on the recrystallization temperatures of the MA956 found in previous works [1,9], a heat treatment was devised at 1285 °C for one hour followed by a furnace cool, a temperature suitable for a subcritical annealing, since it is situated above 0.9 T_m. The purpose of the treatment was stress relief. Previous studies on the MA956 suggested that the only expected phase change at this temperature is the formation of the Cr-rich α'-phase, which takes more than 100 h of isothermal treatment to be formed [10,11]. Therefore, no phase transformation was expected for such a short time interval of exposure to the thermal cycle.

Subsequent to the annealing, a second study of characterisation was carried out, to check for stability of the microstructure. The same techniques (EBSD and TEM) and procedures were deployed, for establishing comparisons between the microstructure and the oxides of the as-received material and of the annealed one. Three TEM foils were prepared, from which another 436 particles from 9 micrographs were analysed.

3. Results

3.1. Microstructure of the as-received MA956

The microscopy survey revealed elongated grains, columnar in shape and strongly oriented along the longitudinal axis of the bars, centimetres in length and several millimetres wide. This is in agreement with the microstructure reported in the literature [12–14].

SEM/EBSD analysis provided further insight into the microstructure. As seen from Fig. 1, the columnar grains, elongated along the extrusion direction, present a strong preferential orientation, mainly characterised by the {100}<110> system, also known as α-fibre; and the {111}<110> system, the γ-fibre. In Fig. 2a, three EBSD maps of adjacent areas of the MA956 microstructure are seen and colour-coded by the IPF contouring, highlighting the fibres, which are confirmed by the Inverse Pole Figures (IPF) shown in Fig. 1b.

Fig. 2 shows the microstructure of the as-received material observed from the cross-section. A distribution function, based on the fraction of high-angle grain boundaries, was obtained from the EBSD and used to estimate the average grain size over four areas of 3750 μm^2, which was found to be 376 ± 48 μm.

3.2. Oxide size distribution – as-received MA956

TEM images show a relatively homogeneous distribution of nanoscale oxides throughout the matrix. In some micrographs, the oxides seem to align with the grain boundaries, reflecting a degree of preferential orientation with the extrusion direction of the material. Fig. 3 illustrates these findings. Some interactions between dislocations and oxide particles were observed. As Fig. 3d portrays, there are some matrix dislocations that seem to have been effectively pinned by the nanometric oxides.

The histogram for size distribution of the oxides is shown in Fig. 4. The average size determined was calculated as 34 ± 7 nm, a value pertaining to the desired range, according to some researchers, for ensuring effectiveness in pinning dislocations [15–17].

3.3. Microstructure of the annealed MA956

Although subjected to a very high temperature, the material did not present any change in its microstructure, which still presents the same features as the original state of the MA956: that is, the α- and γ-fibre textures of the column-like grains, earlier depicted in Figs. 1 and 2. The microstructure of the annealed material is featured in Figs. 5 and 6, in the longitudinal and transverse (cross-sectional) directions, respectively.

While it is known that ferritic grains may grow easily to millimetre size under heat treatments at recrystallization temperatures [18], the results seem to indicate microstructural stability, which is reasonable, considering that the manufactured MA956 already presents columnar grains several centimetres long and hundreds of micrometres wide. There may also be a beneficial pinning effect to the grain boundaries from the oxide dispersion. Estimates of the grain size in the

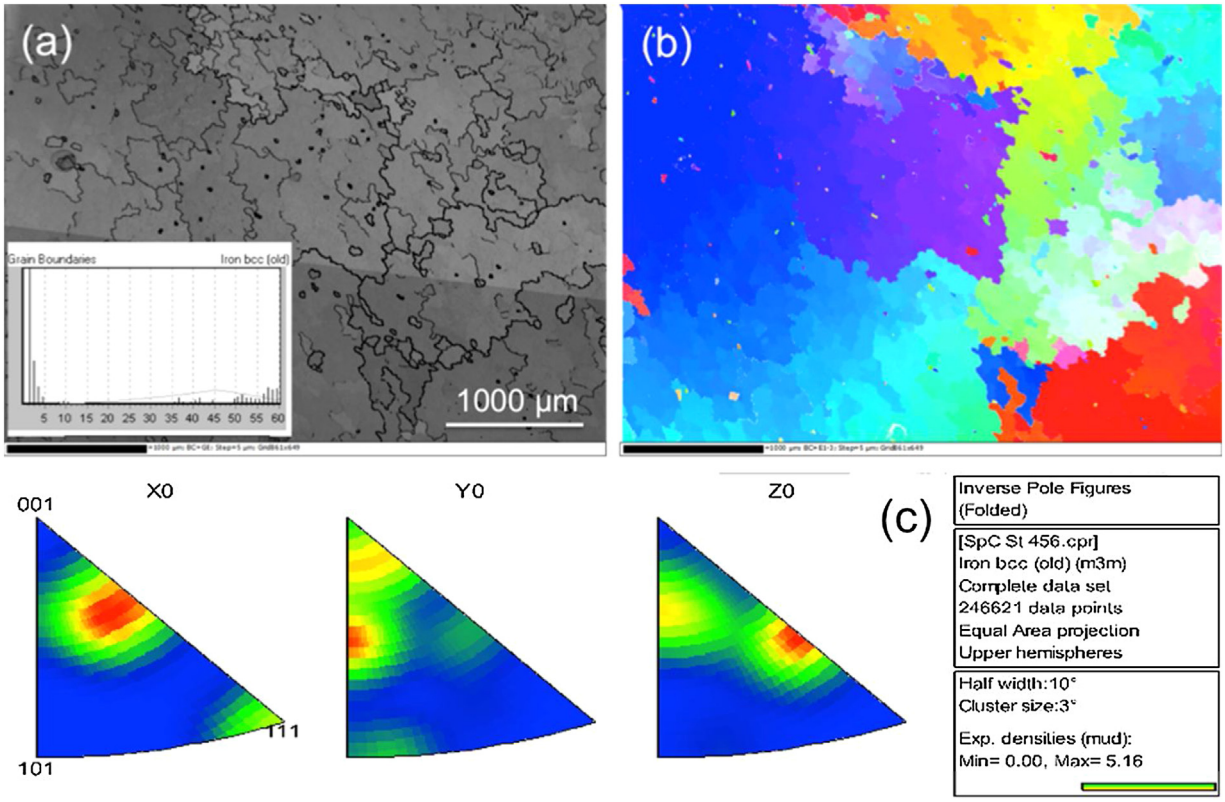

Fig. 2 – Grains observed from the cross-section: (a) grain morphology and distribution of orientations; (b) IPF-coloured grains; and (c) IPF figures showing the distribution of orientations.

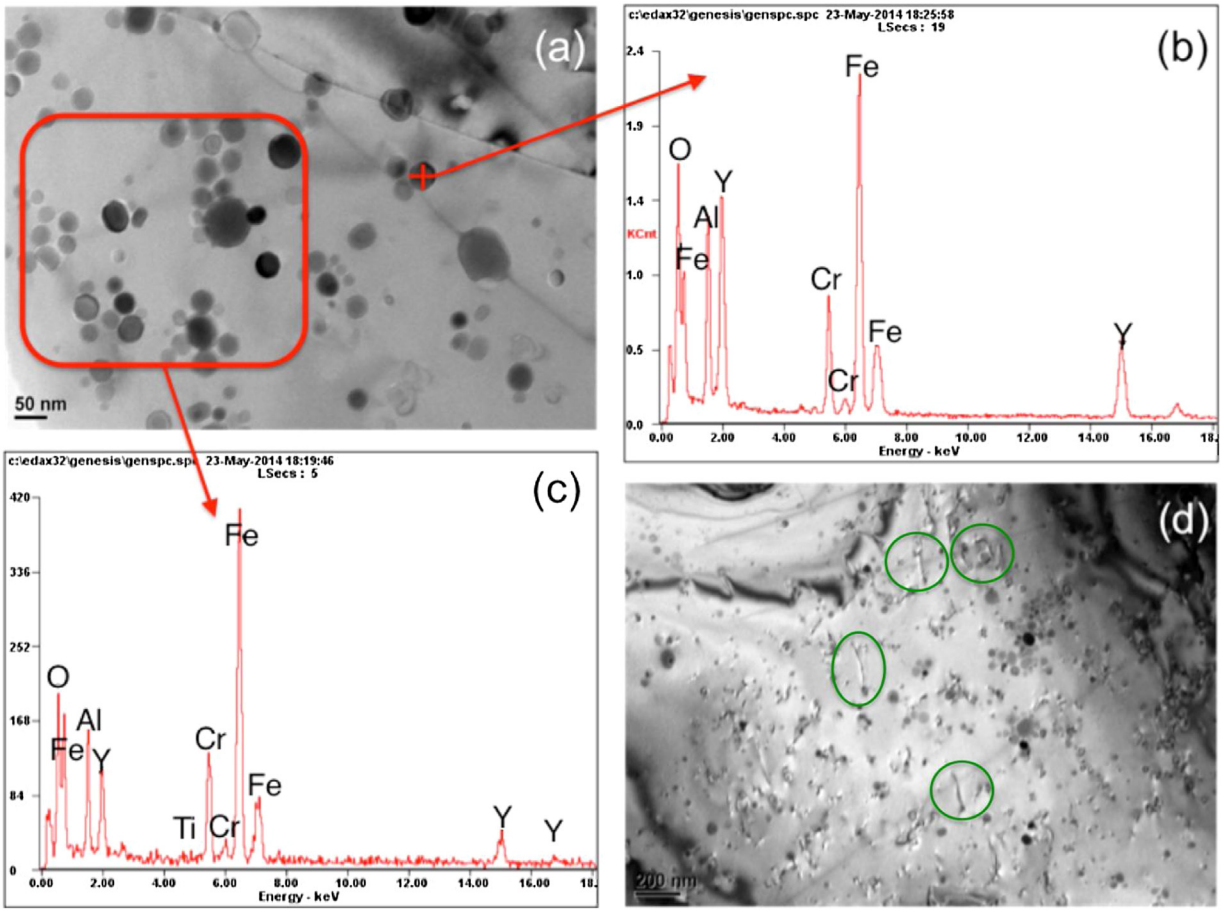

Fig. 3 – TEM micrographs of the as-received MA956. In (a), particles and clusters align with the boundary. (b) and (c) are EDS scans of the indicated targets. (d) shows particles pinning dislocations (highlighted).

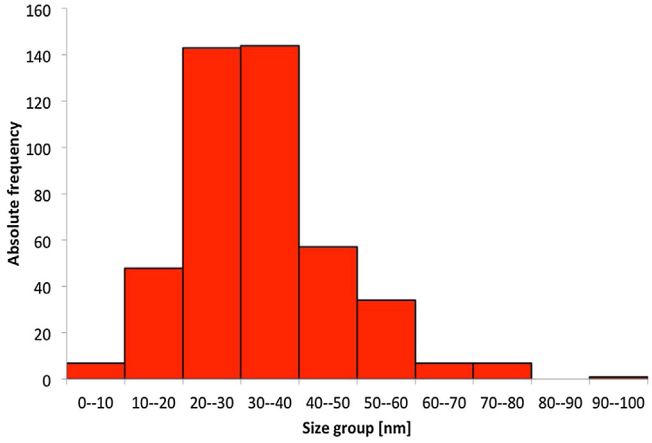

Fig. 4 – Oxide size distribution of the as-received MA956.

cross-sectional direction made from the distribution function averaged 362 ± 39 μm for the grain size. The material, observed from the transverse direction, is seen in Fig. 6.

The TEM investigation on the foils extracted from the annealed material showed an average diameter of 41 ± 8 nm for the oxide particles. The resultant distribution histogram is shown in Fig. 7, where an almost identical distribution to that of Fig. 4 is noticeable.

Given the similarities of the results from the measurements of the oxide particle size, a heteroscedastic student-t test (that is, a test designed with the assumption of unequal variances) was carried out with a significance probability of 5%, having the null hypothesis stating that no significant difference exists between the oxide size distribution in the as-received material and in the heat-treated one. For the number of degrees of freedom associated with the sample size of the oxides, the critical t-value of the probability for acceptance of the null hypothesis was determined as 1.96. The t-value calculated for the test reached 5.08, a much higher than the maximum value for affirming, with 95% confidence, that the two size distributions are equivalent. The rejection of the null hypothesis, then, means that, statistically, differences between the oxide distributions in the as-received and the annealed MA956 exist and are measurable. Summarised details of the conducted hypothesis test are found in Table 2.

4. Discussion

Part of the interest around ODS materials stems from claims of the stability of the oxides. The possibility of taking the

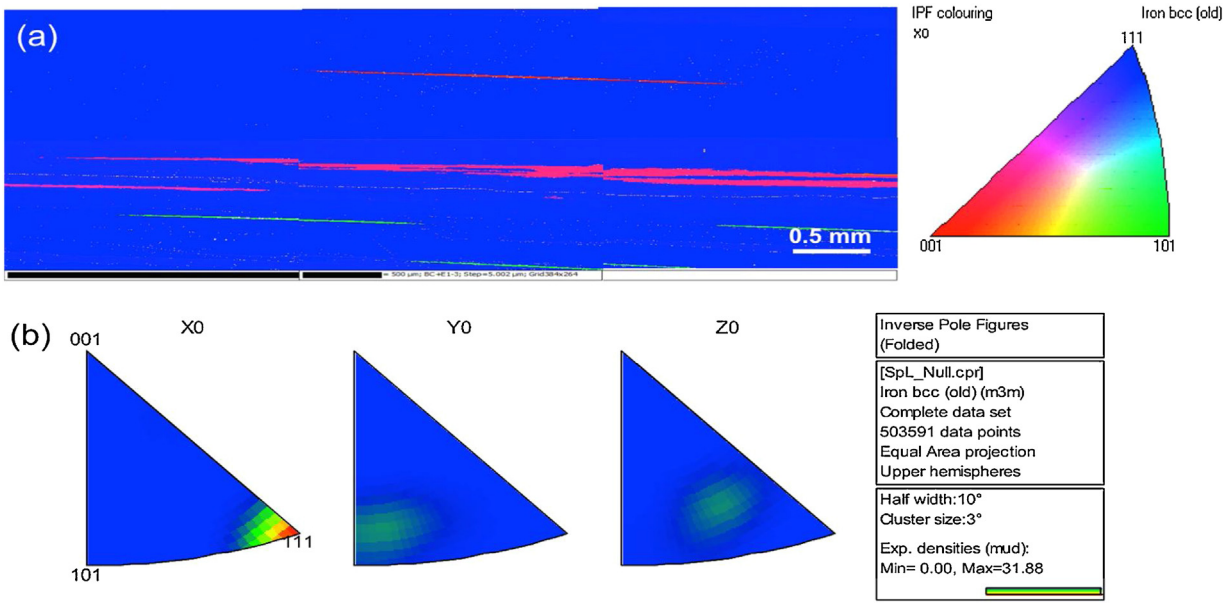

Fig. 5 – EBSD map of the annealed MA956 in the longitudinal direction (a); the IPF figures indicate the predominance of the same fibre orientations as observed for the as-received material (b).

material to much higher temperatures than conventional materials, reaching temperatures near the melting point, but still retaining the configuration of the dispersoids, has been verified as a fundamental asset. Noh and co-workers reported stability of the oxides in diffusion bonding cycles reaching temperatures as high as 1200 °C [19,20]; Sittel et al. [21] found no difference in the oxide side distribution of PM2000 ferritic steel subject to diffusion bonding cycles at 1100 °C and 1300 °C.

Other studies provide support to the notion of stable oxides in harsh environments [22,23]. However, the common point in all these investigations is the fact that the oxides studied were complex Y-Ti-O oxides. Titanium has been defined as an effective refiner of the oxides in the matrix [8,24,25]. Aluminium, although also used for refining the primary Y_2O_3 oxide, does not have the same effect as Ti, and heat treatments at high temperatures (above 1100 °C) during fabrication of the alloy

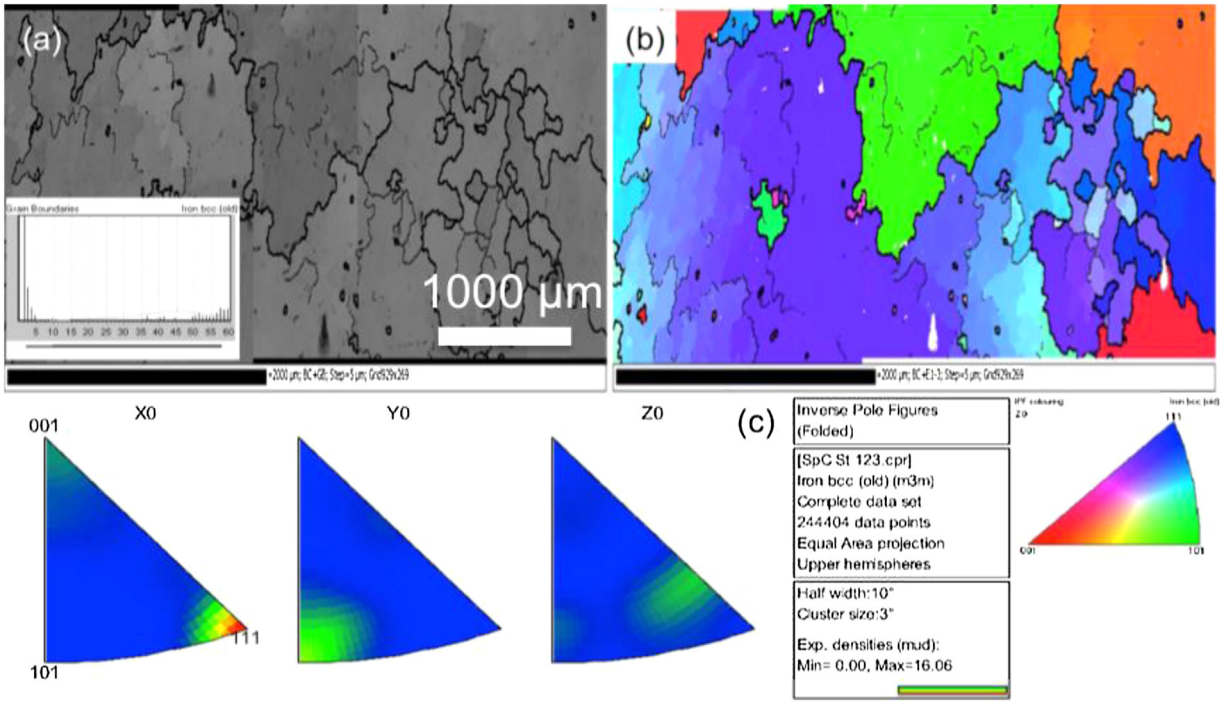

Fig. 6 – EBSD map of heat-treated cross-sectional MA956. (a) grain morphology and distribution of orientation. (b) The same grains, but IPF-coloured; (c) the IPF figures corresponding to the micrograph.

Table 2 – Hypothesis test summary and details for the means of the oxide size distributions — as-received and annealed MA956.

Sample	No. of particles	Mean particle size	Standard Deviation
As-received	449	34.2	18.1
Heat-treated	436	41.1	22.3
t-test assuming unequal variances (heteroscedastic)		two-tailed distribution	
Degrees of Freedom	838	Critical Value (5%)	1.96
Hypothesized Mean Difference	0		
Pooled Variance	411.68	Status of the null hypothesis	Rejected
Test Statistics	5.08		

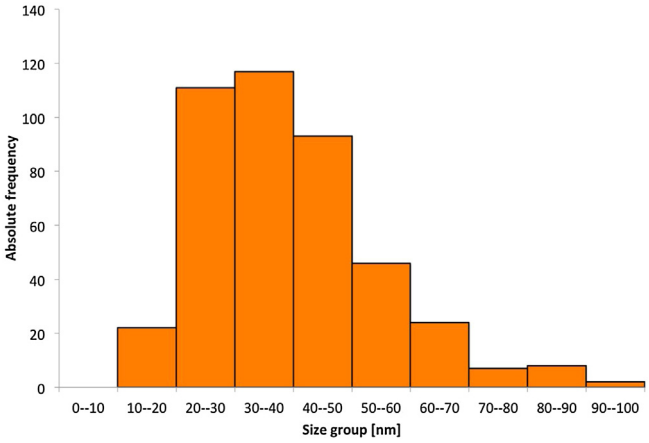

Fig. 7 – Oxide size distribution for the heat-treated (1285 °C/1 h) MA956.

render the complex Y-Al-O oxides coarser than those of the Y-Ti-O group [24]. Moreover, when aluminium is part of a steel composition in higher amounts, compared to titanium, Y-Al-O oxides are formed over the more stable Y-Ti-O complex oxides [26]. While the present work cannot determine whether the oxides in the MA956 belong exclusively to the Y-Al-O complex, a number of authors indicate the predominance of such oxides in the material, more specifically, yttrium-aluminium-perovskite, YAP ($YAlO_3$) [2], yttrium-aluminium-garnet, YAG ($Y_3Al_5O_{12}$) [3,14]; and yttrium-aluminium-monoclinic, YAM ($Y_4Al_2O_9$) [27], owing to the high affinity between aluminium and oxygen.

A visual comparison of Figs. 4 and 7 allows the conclusion that the particles grew slightly. The hypothesis test provided a statistical basis for this observation. The results of this investigation, along with the considerations found in the literature, indicate that, even if a further degree of refinement of the yttria can be achieved in Al-added alloys, as a result of, for example, a more controlled manufacturing process in which particles of the powders are exposed to more violent fragmentation, the Y-Al-O oxides will not retain their size, if exposed to high temperature treatments and processes. This finds agreement with a recent investigation by Zhang and Pantleon [28], who reported significant growth of the YAP oxides from 14 nm to approximately 19 nm, 25 nm and 28 nm after annealing the ODS FeCrAl steel PM2000 at 1300 °C for 1, 10 and 100 h, respectively.

The stability of the oxide particles under harsh conditions or high temperature thermal cycles seems to be ultimately related to the chemical composition of the oxides. Therefore, investigations on the stability of oxides should not only look into the transformations during the manufacturing stages, but, also, during later exposure to high temperature processes. Given that many elements are added in an effort to produce finer oxides in the matrix [6,29], further studies are required to check for stable dispersoids at high temperatures in post-manufacturing processes.

A question that may arise from the findings of the work presented regards the mechanisms for growth of the oxides. This has not been investigated, but, given the very high temperature of the heat treatment, the high contents of aluminium and the presence of oxygen dissolved in the matrix, diffusion of these elements to the oxide, changing its stoichiometric proportions is plausible. Another possible way is attributed to Ostwald ripening, that is, a decrease of the total energy of the system by elimination of interfaces, as growth takes place at the expense of the volume fractions of smaller particles [30]. Such an investigation, however, would also have to rely on mean particle spacing and particle density measure in the two conditions.

Finally, it may well be the case that the thermal cycle affected the grain structure. A hypothesis test would be required to check the equivalence between the averages determined from the population of grains in each condition. However, the focus of the analysis has been set on the oxides, which constitute the main strengthening features of the ODS alloys.

5. Conclusions

1 Heat treatment at 1285 °C on the MA956 ferritic ODS steel caused the nanometric dispersed oxides to grow slightly. A shift in the size distribution was observed, when comparing the as-received material to the annealed version. A hypothesis test provided support to the observed differences between the particles, which grew from an average of 34 nm to an average of 41 nm with the heat treatment.
2 The Y-Al-O complex oxides are found not to be as stable as has previously been suggested in the literature. Based on these results and previous studies, oxides formed with titanium appear less prone to growth under thermal treatment.
3 Even if the manufacturing process is capable of producing refined oxides in the MA956, exposure to high temperature processes causes the oxides to grow, which may result in loss of effectiveness in pinning dislocations and entrapping defects.

Conflicts of interest

The authors declare no conflicts of interest.

Acknowledgements

JROL was funded through the RCUK Energy Programme, and we are grateful to EPSRC for funding via the PROMINENT Nuclear Fission consortium grant. MEF is grateful for funding from the Lloyd's Register Foundation, a charitable foundation helping to protect life and property by supporting engineering-related education, public engagement and the application of research.

REFERENCES

[1] Bhadeshia HKDH. Recrystallization of practical mechanically alloyed Iron-base and Nickel-base Superalloys. Mater Sci Eng A 1997;223:64–77.
[2] Czyrska-Filemonowicz A, Szot K, Wasilkowska A, Gil A, Quadakkers WJ. Microscopy (AFM, TEM, SEM) studies of oxide scale formation on FeCrAl based ODS alloys. Solid State Ion 1999;117(February (1-2)):13–20.
[3] Dubiel B, Osuch W, Wróbel M, Ennis PJ, Czyrska-Filemonowicz A. Correlation of the microstructure and the tensile deformation of incoloy MA956. J Mater Process Technol 1995;53:121–30.
[4] Chen J, Jung P, Pouchon MA, Rebac T, Hoffelner W. Irradiation creep and precipitation in a ferritic ODS steel under helium implantation. J. Nucl. Mater.3731 2008;373(1-3): 22–7.
[5] Toloczko MB, Gelles DS, Garner FA, Kurtz RJ, Abe K. Irradiation creep and swelling from 400 to 600 °C of the oxide dispersion strengthened ferritic alloy MA957. J. Nucl. Mater 2004;329–333(0):352–5.
[6] Oka H, Watanabe M, Ohnuki S, Hashimoto N, Yamashita S, Ohtsuka S. Effects of milling process and alloying additions on oxide particle dispersion in austenitic stainless steel. J. Nucl. Mater 2014;447:248–53.
[7] Schaffer GB, Loretto MH, Smallman RE, Brooks JW. The stability of the oxide dispersion in INCONEL alloy MA6000. Acta Metall 1989;37(September (9)):2551–8.
[8] Zakine C, Prioul C, François D. Creep behaviour of ODS steels. Mater Sci Eng A 1996;219(1-2):102–8.
[9] Betz W, Brunetaud R, Coutsouradis D, Fischmeister H, Gibbons TB, Kvernes I, et al. High temperature alloys for gas turbines and other applications. D. Reidel Publishing Company; 1986.
[10] Chao J, González-Carrasco JL, Capdevilla C. Influence of annealing at 1100°C and 475°C on the mechanical properties at room temperature of an Iron base ODS alloy. ISIJ Int 2007;47:1214–20.
[11] Capdevila C, Miller MK, Toda I, Chao J. Influence of the α–α′ phase separation on the tensile properties of Fe-base ODS PM 2000 alloy. Mater Sci Eng A 2010;527(November (29-30)):7931–8.
[12] Czyrska-Filemonowicz A, Wróbel M, Dubiel B, Ennis PJ. Transmission electron micriscopy study of dislocation-dispersoid interaction in deformed Incoloy MA956. Scr Metall Mater 1995;32(3):331–5.
[13] Wasilkowska A, Bartsch M, Messerschmidt U, Herzog R, Czyrska-Filemonowicz A. Creep mechanisms of ferritic oxide dispersion strengthened alloys. J Mater Process Technol 2003;133(February (1-2)):218–24.
[14] Dubiel EL, Wróbel M, Ennis PJ, Czyrska-Filemonowicz A. Microstructure of Incoloy MA956 after low and high temperature deformation. Scr Mater 1997;37(8):1215–20.
[15] Wolski K, Thévenot F, Le Coze J. Effect of nanometric oxide dispersion on creep resistance of ODS-FeAl prepared by mechanical alloying. Intermet A 1996;4:299–307.
[16] Rösler J, Arzt E. A new model-based creep equation for dispersion strengthened materials. Acta Metall Mater 1990;38(4):671–83.
[17] Arzt E. Creep of oxide-dispersion strengthened alloys. In: Encyclopedia of materials: science and technology. Elsevier; 2001. p. 1800–6.
[18] Klueh RL, Harries DR. High-chromium ferritic and martensitic steels for nuclear applications. American Society for Testing and Materials; 2001.
[19] Noh S, Kasada R, Kimura A. Solid-state diffusion bonding of high-Cr ODS ferritic steel. Acta Mater 2011;59(8):3196–204.
[20] Noh S, Kim B, Kasada R, Kimura A. Diffusion bonding between ODS ferritic steel and F82H steel for fusion applications. J. Nucl. Mater.4261– 2012;426(1-3):208–13.
[21] Sittel W, Basuki WW, Aktaa J. Diffusion bonding of the oxide dispersion strengthened steel PM2000. J. Nucl. Mater.4431–2013;443(1-3):78–83.
[22] Chen J, Pouchon MA, Kimura A, Jung P, Hoffelner W. Irradiation creep and microstructural changes in an advanced ODS ferritic steel during helium implantation under stress. J. Nucl. Mater 2009;386–388(0):143–6.
[23] Noh S, Kasada R, Oono N, Iwata N, Kimura A. Evaluation of microstructure and mechanical properties of liquid phase diffusion bonded ODS steels. Fusion Eng Des 2010;85(7-9):1033–7.
[24] Kasada R, Toda N, Yutani K, Cho HS, Kishimoto H, Kimura A. Pre- and post-deformation microstructures of oxide dispersion strengthened ferritic steels. J. Nucl. Mater.367–370 2007;367–370(August):222–8.
[25] Ratti M, Leuvrey D, Mathon MH, de Carlan Y. Influence of titanium on nano-cluster (Y, Ti, O) stability in ODS ferritic materials. J. Nucl. Mater 2009;386-388:540–3.
[26] Lee JH. Development of oxide dispersion strengthened ferritic steels with and without aluminum. Front Energy 2012;6(March (1)):29–34.
[27] Hsiung LL, Fluss MJ, Tumey SJ, Choi BW, Serruys Y, Willaime F, et al. Formation mechanism and the role of nanoparticles in Fe-Cr ODS steels developed for radiation tolerance. Phys Rev B 2010;82(November (18)):184103.
[28] Zhang Z, Pantleon W. Oxide nanoparticles in an Al-alloyed oxide dispersion strengthened steel: crystallographic structure and interface with ferrite matrix. Philos Mag (Abingdon) 2017;97(21):1824–46.
[29] Oka H, Watanabe M, Hashimoto N, Ohnuki S, Yamashita S, Ohtsuka S. Morphology of oxide particles in ODS austenitic stainless steel. J. Nucl. Mater.4421–3 2013;442(November (1-3)):S164–8.
[30] Krautwasser P, Czyrska-Filemonowicz A, Widera M, Carsughi F. Thermal stability of dispersoids in ferritic oxide-dispersion-strengthened alloys. Mater Sci Eng A 1994;177(April (1-2)):199–208.